IDENTIFYING ELECTRONIC PROPERTIES RELEVANT TO IMPROVING THE PERFORMANCE AND STABILITY OF AMORPHOUS SILICON BASED PHOTOVOLTAIC CELLS

Annual Subcontract Report 27 November 2002- 26 November 2003

J. David Cohen
Department of Physics and Materials Science Institute
University of Oregon, Eugene, Oregon

Prepared for the National Renewable Energy Laboratory

under Subcontract No. ADJ-2-30630-17

NREL Technical Monitor: B. von Roedern

PREFACE

This Annual Technical Progress Report covers the work performed at the University of Oregon for the period 27 November 2002- 26 November 2003 under NREL Subcontract Number ADJ-2-30630-17. The following personnel participated in this research program:

NAME	TITLE	WORK PERFORMED
J. David Cohen	Principal Investigator	Program Manager
James Gutierrez	Research Assistant	Properties of Iowa State a- Ge:H samples and United Solar nanocrystalline Si materials
Adam Halverson	Research Assistant	Properties of United Solar nanocrystalline Si material

TABLE OF CONTENTS

Page

LIST OF ILLUSTRATIONS iv

LIST OF TABLES iv

EXECUTIVE SUMMARY v

1.0 INTRODUCTION 1

2.0 SAMPLES

2.1 IOWA STATE AMORPHOUS GERMANIUM 1
2.2 UNITED SOLAR NANOCRYSTALLINE SILICON 2

3.0 EXPERIMENTAL CHARACTERIZATION METHODS

3.1 ADMITTANCE SPECTROSCOPY 3
3.2 DRIVE-LEVEL CAPACITANCE PROFILING 4
3.3 TRANSIENT PHOTOCAPACITANCE AND PHOTOCURRENT 4

4.0 ELECTRONIC PROPERTIES OF ECR DEPOSITED AMORPHOUS GERMANIUM 7

5.0 PROPERTIES OF UNITED SOLAR NANOCRYSTALLINE SILICON 8

5.1 ADMITTANCE AND DRIVE-LEVEL CAPACITANCE PROFILING STUDIES 9
5.2 SUB-BAND-GAP PHOTOCAPACITANCE SPECTROSCOPY 11
5.3 LIGHT INDUCED EFFECTS IN MICROCRYSTALLINE SILICON 13

6.0 SUMMARY AND CONCLUSIONS 15

7.0 SUBCONTRACT SUPPORTED PUBLICATIONS 17

8.0 REFERENCES 17

LIST OF ILLUSTRATIONS

Page

FIG. 1(a) Capacitance and conductance vs. temperature for Iowa State a-Ge:H
1(b) Arrhenius plot of the inflection points of the capacitance step vs. frequency 2

FIG. 2. Schematic of four different types of sub-bandgap optical transitions 5

FIG. 3 Drive-level capacitance profiles of a-Ge:H taken at 330Hz
at three measurement temperatures 7

FIG. 4. Transient photocapacitance and transient junction photocurrent spectra
for Iowas State a-Ge:H sample 6059 8

FIG. 5. Variation of the junction capacitance with voltage for the 14140
a-Si:H/nc-Si:H/a-Si:H sandwich sample..... 9

FIG. 6(a) Capacitance vs. temperature for one multilayer sample at 7 measurement frequencies
6(b) Arrhenius plot of capacitance step reveals an activation energy near 0.5eV..... 10

FIG. 7. DLCP curves for the pin nc-Si:H device 11

FIG. 8. DLCP curves for the a-Si:H/nc-Si:H/a-Si:H multilayer sample 14140 11

FIG. 9. CPM spectrum for μc-Si:H taken from the paper by M. Vaneček et al..... 12

FIG. 10. TPC spectra for one sandwich nc-Si:H sample device
at three measurement temperatures 12

FIG. 11. Photocapacitance spectra for one a-Si:H/nc-Si:H/a-Si:H multilayer sample
at two measurement temperatures 13

FIG. 12. Photocapacitance spectra for the pin nc-Si:H device
at two measurement temperatures 13

FIG. 13(a) 200K TPC spectra in State A and after 2 periods of light soaking
13(b) 280K TPC spectra in State A and after 2 periods of light soaking 14

FIG. 14 Drive-level capacitance profiles taken at 1.1kHz and 320K for State A
and various stages of light soaking 15

LIST OF TABLES

TABLE I. United Solar nc-Si:H samples studied during this Subcontract year. 3

EXECUTIVE SUMMARY

During this second phase of our NREL Subcontract period we have focused primarily upon the characterization of hydrogenated nanocrystalline Si (nc-Si:H) produced at United Solar Ovonics Corporation. In addition, we examined a couple of amorphous germanium (a-Ge:H) samples produced by the ECR method at Iowa State University. Our studies of the ECR a-Ge:H confirmed the superior electronic properties of the Iowa State a-Ge:H material, both in terms of the DLCP deduced defect densities, and the TPC deduced Urbach energies.

In our studies of the USOC nc-Si:H samples we found DLCP state densities in the 10^{15} to 10^{16} cm^{-3} range. Very little temperature dependence was observed, indicating that the majority of these are shallow donor-like states. For all 3 samples studied we observed that the DLCP densities increased in the direction of film growth. This is consistent with observations at USOC that the crystallinity size increases as the films become thicker. Our transient photocapacitance measurements disclosed a sub-band-gap spectrum that evolved from a very μc-Si:H appearance at lower temperatures (200K), to a very a-Si:H like in appearance at moderate temperatures (300K). We believe this change in appearance results from improving hole carrier collection as the temperature is increased which then diminishes the photocapacitance response of the nc-Si:H component in these materials. However, the hole carrier collection remains relatively poor in the a-Si:H component in these nc-Si:H samples so that the TPC signal in that component thus becomes dominant in the higher temperature regime even though its volume fraction is undoubtedly fairly small. Thus, our TPC method allows us to examine the electronic properties of both components in these mixed phase materials.

Finally, we have begun to examine the effects of light-induced degradation in these nc-Si:H materials. The DLCP measurements actually showed very little change with light soaking, even after 100 hours at $100mW/cm^2$. However, significant degradation in the hole carrier collection properties were observed in the TPC measurements. However, we did not any increase in any specific spectral feature or defect band that might provide a clue for a mechanism that might be responsible for this reduction in hole collection.

1.0 INTRODUCTION

The work carried out in Phase II under NREL Subcontract ADJ-2-30630-17 has concentrated on two types of studies. First, we examined a-Ge:H samples prepared in Vikram Dalal's laboratory at Iowa State University. Using their ECR growth technique and a very high degree of hydrogen and/or helium dilution, they have recently reported high Ge fraction a-Si,Ge:H material with good electronic properties as well as solar cell devices with fill factors in excess of 0.6 for alloys with Tauc gaps below 1.4eV.[1] To help verify the superior electronic properties of this material my laboratory characterized the electronic properties of a couple samples of their pure a-Ge:H material.

Second, we began an evaluation of the microcrystalline Si material currently being developed by scientists at United Solar Ovonics Corporation (USOC). Because this material is actually a hydrogenated nanocrystalline form of Si it will be denoted in this report as nc-Si:H. It is hoped that such a material may ultimately be able to replace one of a-Si,Ge:H layers in an amorphous silicon triple junction device. Initially it had been found that these films were particularly susceptible to post-deposition oxygen contamination. This could be prevented by depositing capping layers of a-Si:H. Thus, we obtained two samples in a sandwich configuration (nc-Si:H between two thinner a-Si:H layers), but included one p-i-n nc-Si:H sample for comparison.

In the Sections that follow, we first describe the samples studied and then briefly review the experimental techniques employed. In Section 4 we discuss our results concerning the a-Ge:H material obtained from Iowa State. In Section 5 we present our preliminary results on the nc-Si:H material obtained from USOC. Finally, in Section 6 we will summarize our findings and try to draw some general conclusions.

2.0 SAMPLES

2.1 IOWA STATE AMORPHOUS GERMANIUM

We obtained a couple a-Ge:H samples prepared in Vikram Dalal's laboratory at Iowa State University that were depostion using their ECR growth technique. These samples were deposited in a "half-device" sample configuration: SS/n^+/a-Ge:H. The a-Ge:H films were deposited at 260-270^{o}C with a H_2:GeH_4 dilution ratio of 100:1. The a-Ge:H film thickness was 0.3μm. Our test devices were completed by depositing Cr Schottky barrier contacts on the top surface.

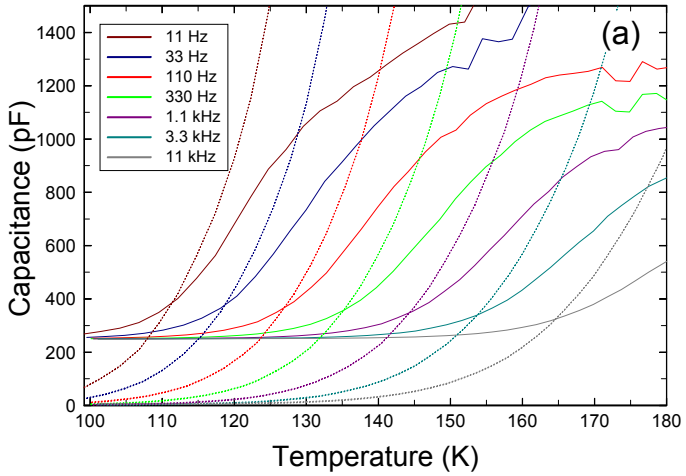

FIG. 1(a). Capacitance (solid lines) and conductance (dotted lines) vs. temperature for Iowa State a-Ge:H sample 6059 at 0V applied bias at seven measurement frequencies.

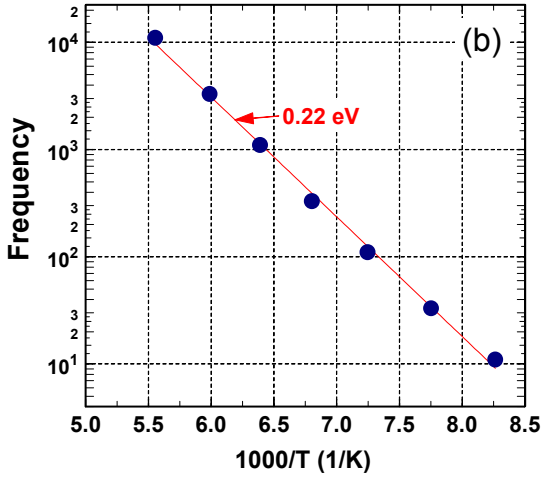

FIG. 1(b). Arrhenius plot of the inflection points of the capacitance step vs. frequency displayed in Fig. 1(a) reveals the activation energy of conductivity.

Initially we had some difficulty identifying a metal for the top contact that would lead to a good Schottky barrier. Our usual choice for a-Si,Ge:H alloy samples in the past was Pd; however, these did not produce good blocking contacts. Ultimately, we found that Cr contacts produced usable, but somewhat leaky, Schottky barriers. An admittance scan (capacitance and conductance vs. temperature) is displayed in Fig. 1(a). This set of data reveals a well-defined junction capacitance; however, the conductance is rather large at all frequencies. This means that some extra care needed to be taken to separate the capacitance and conductance phases of the current response. The step increase in the capacitance is thermally activated (see Fig. 1(b)) and discloses the conductivity activation energy for this a-Ge:H sample (about 0.22 eV).

2.2 UNITED SOLAR NANOCRYSTALLINE SILICON

All the nc-Si:H devices studied during this period were fabricated at United Solar. They are listed in Table I. A purely nc-Si:H p-i-n device containing a 1000 nm intrinsic layer had a SS/n^+/i/p^+/TCO structure. The two sandwich devices consisted of roughly 700nm thick nc-Si:H layers clad between two 200 to 250nm thick a-Si:H layers in a SS/n+/a-Si:H/nc-Si:H/a-Si:H structure. These two samples were grown using different levels of hydrogen dilution. We deposited a Pd Schottky barrier on top of each such sandwich sample device for our measurements.

There are a couple reasons for fabricating and characterizing nc-Si:H in these two different device structures (sandwich vs. pin). First, we wanted to discriminate against effects of

Table I. United Solar nc-Si:H samples studied during this Subcontract year.

Sample #	Device Type	nc-Si:H thickness (nm)	Hydrogen Dilution	a-Si:H layer thickness (nm)
14140	Sandwich	770	Standard	2x250
14657	Sandwich	640	25% Less	2x250
12123	p-i-n	1000	Standard	None

possible oxygen contamination of the nc-Si:H which are inhibited by the a-Si:H cladding layers in the sandwich structure. However, we also wanted to understand any possible effects of the a-Si:H layers on our results. We expect these layers to behave only as insulating layers in our measurements provided we work at sufficiently low temperatures. Results on the p-i-n structure can be used to check this since it only contains nc-Si:H. However, the p-i-n sample also contains heavily doped n and p layers which may also partially obscure the response due to the intrinsic layer itself.

3.0 EXPERIMENTAL CHARACTERIZATION METHODS

The measurements employed in our studies rely on a set of experimental techniques which have all been described previously in some detail. They consist of (1) admittance spectroscopy as a function of temperature and frequency, (2) drive-level capacitance profiling, and (3) transient photocapacitance taken together with transient junction photocurrent spectroscopy. Here we will describe each method only very briefly and review what kind of information is obtained from each type of measurement.

3.1 ADMITTANCE SPECTROSCOPY

Our Schottky diode samples contain a depletion region which is characterized as a function of temperature and frequency [see, for example, Fig. 1] before we undertake the more sophisticated capacitance based measurements described in Sections 3.2 and 3.3 below. Such measurements provide us with an estimate of our film thickness (the temperature independent region at low T is simply related to the geometric thickness, d, by the formula $C = \varepsilon A/d$), and an Arrhenius plot of the frequency of the lowest temperature capacitance step (or conductance peak) *vs*. 1/T provides us with the activation energy of the ac conductivity, E_σ, which we identify with the Fermi energy position: $E_\sigma = E_C - E_F$.[2] These admittance measurements also give us an indication of the quality of our Schottky barriers which allow us to pre-screen our samples for further study.

3.2 DRIVE-LEVEL CAPACITANCE PROFILING

The drive-level capacitance profiling method has been described in detail in many publications [3,4]. It is similar to other kinds of capacitance profiling in that it provides us with a density *vs*. distance profile; however, this particular method was developed specifically to address the difficulties encountered in interpreting capacitance measurements in materials with defect densities comparable to carrier densities. In this method we monitor the junction capacitance both as a function of DC bias, V_B, and as a function of the amplitude of the alternating exciting voltage, δV. One finds that to lowest order this dependence obeys an equation of the form:

$$C(V_B,\delta V) = C_o(V_B) + C_1(V_B)\,\delta V + \ldots$$

and that the ratio

$$N_{DL} \equiv \frac{C_0^3}{2q_e \varepsilon A^2 C_1} \tag{1}$$

is directly related to the free carrier density, n, plus an integral over the density of mobility gap defect states:

$$N_{DL} = n + \int_{E_c - E_e}^{E_F^o} g(E)dE \tag{2}$$

Here E_F^o is the bulk Fermi level position in the sample and E_e depends on the frequency and temperature of measurement:

$$E_e(\omega,T) = k_B T \log(\nu/\omega) \tag{3}$$

Thus, by altering the measurement temperature (or frequency) we obtain information about the energy distribution of the defects and, by altering the applied DC bias, we can vary the spatial region at which we detect the defects in the sample. That is, we can spatially profile the defects as a function of the position from the barrier interface.

3.3 TRANSIENT PHOTOCAPACITANCE AND PHOTOCURRENT

The methods of junction transient photocapacitance and photocurrent have been discussed by us in great detail over the years in the literature [5,6,7] and also in previous NREL reports. They represent types of sub-band-gap optical spectroscopy and provide spectra quite similar in appearance to PDS derived sub-band-gap optical absorption spectra or to CPM spectra. Instead

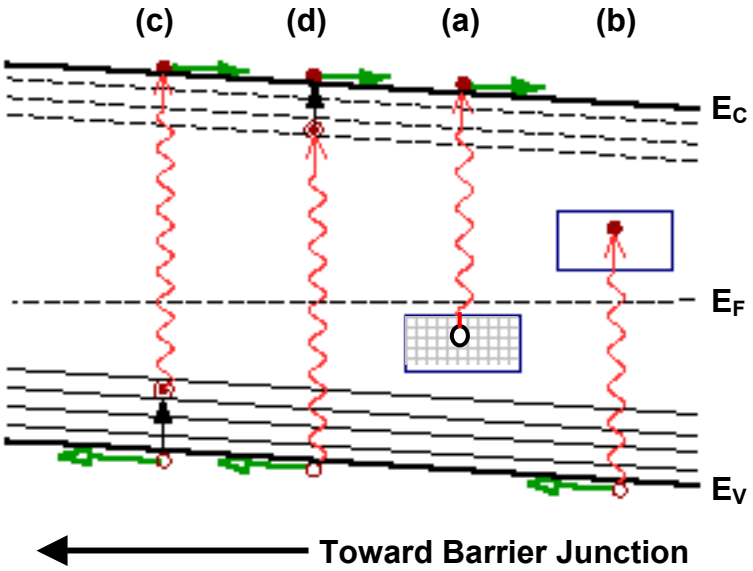

FIG. 2. Schematic of four different types of sub-bandgap optical transitions. Optical tran-sitions are shown by the wavy lines, and thermal transitions are shown by the vertical solid arrows. Horizontal arrows indicate the subsequent motion of the released carriers.

of detecting absorbed energy, however, our photocapacitance and photocurrent transient methods detect the optically induced change in defect charge within the depletion region.

In this method the space charge region of the semiconductor near the barrier junction is first subjected to a voltage "filling pulse". This pulse causes a non-equilibrium (filled) occupation of gap states to be established. As time progresses, the initial steady-state population is recovered through the excitation of trapped electrons to the conduction band where they can then move out of the depletion region under the influence of the electric field. In the dark this process proceeds entirely by the thermal excitation of trapped carriers. However, this process can be enhanced through optical excitation and this is the basis of the photocapacitance and junction photocurrent techniques.

The re-equilibration can be observed by the redistribution of trapped carriers, either as a change in the *junction capacitance* (which occurs because the depletion region will contract as negative charge is lost and the positive charge density increases) or by monitoring the *current* which results from the motion of this charge. However, the observation of capacitance transients has one significant difference compared to current transient measurements: The dominant type of emitted carrier (electron or hole) can be identified by the *sign* of the observed change in capacitance.

Unlike the CPM method, both of our junction based techniques are not greatly influenced by the free carrier mobilities since, once an electron (or hole) is optically excited into the conduction (valence) band it will either totally escape the depletion region on the slow timescale

of our measurement (0.1 to 1s) or be retrapped into a deep state and not escape. In most cases we assume that almost all of the optically excited majority carriers (electrons) *do* escape but, in general, only a fraction of the minority carriers (holes).

In Figure 2 we have separated the types of optical transitions involving gap states into four types.[8] Type (a) is the removal of an electron from an occupied defect level into the conduction band with the subsequent escape of the electron. Type (b) represents the optical excitation between the valence band and an unoccupied defect states with the subsequent escape of the valence band hole. Such a transition results in a photocapacitance signal of negative sign. Generally, such negative photocapacitance signals occur only in very intrinsic material and are even fairly rare in those cases. They have been most prominently observed in some a-Si,Ge:H samples [9], and in some mixed phase a-Si:H / nc-Si:H samples [10].

Transitions of type (c) are similar to type (a) except that, because the hole left in the gap state lies close to the valence band, it will be quickly thermally emitted into the valence band where it then also escapes the depletion region. Such a case results in no change in charge state within the depletion and, hence, no photocapacitance signal. Similarly, [Type (d)] for a transition from the valence band into an unoccupied gap state close to the conduction band, the electron will be quickly thermally emitted into the conduction band and leave the depletion region as well, with nearly zero photocapacitance signal.

We expect that transitions of types (c) and (d) will be dominant when the photon energy lies only slightly below the bandgap energy. For such transitions each photon effectively produces one valence band hole plus one conduction band electron with no net change in the gap state occupation. However, we generally find that the photocapacitance signal in this energy regime does not vanish; rather, it is substantially *positive*. This thus indicates that photogenerated electrons are more likely to escape the depletion region than photogenerated holes. Moreover, while transitions of types (c) and (d) result in small changes in the junction capacitance, they result in a large junction photocurrent.

In general terms, if our sub-bandgap light results in n_e electrons and n_h holes leaving the depletion within the experimental time window, then the junction photocurrent signal will be proportional to $n_e + n_h$, while the photocapacitance signal will be proportional to $n_e - n_h$. Thus, it is really only by measurements of *both* the transient photocapacitance (TPC) signal *as well as* the transient photocurrent (TPI) signal that we can truly distinguish the quantities of holes and electrons excited out of the depletion region due to the sub-bandgap light. This ability to distinguish electron from hole processes is unique among all the various types of sub-band-gap optical spectroscopies.

4.0 ELECTRONIC PROPERTIES OF ECR DEPOSITED AMORPHOUS GERMANIUM

We characterized the a-Ge:H material deposited at Iowa State University using the ECR method by employing the drive-level capacitance profiling (DLCP) technique, and transient photocapacitance (TPC) spectroscopy, as described in Section 3 above. A series of 330Hz drive-level profiles is shown in Fig. 3 and indicates defect densities near the mid 10^{16} cm^{-3} level. The fact that these profiles do not change appreciably with temperature indicates that these defects must lie fairly close to the conduction band mobility edge. Specifically, to respond at 180K to the 330Hz oscillating voltage indicates an activation of less than 0.4eV.

In Fig. 4 we display both a transient photocapacitance and a junction transient photocurrent spectrum for this a-Ge:H sample. Both spectra are nearly identical and indicate a 42 meV Urbach energy and a defect band shoulder consistent with the DLCP estimate of a mid 10^{16} cm^{-3} defect density for this sample. These spectra also indicate an optical (E_{04}) optical gap of roughly 1.3eV. Such a narrow bandtail and low defect density indicate that this a-Ge:H material is of the highest quality. Indeed, it appears superior to all such samples we have measured with the possible exception of the Harvard cathodic glow discharge a-Ge:H samples.[11] In addition, the indicated high quality of these electronic properties is reflected in the excellent performance of the solar cell devices that has recently been demonstrated by the Dalal group for these alloy materials [1].

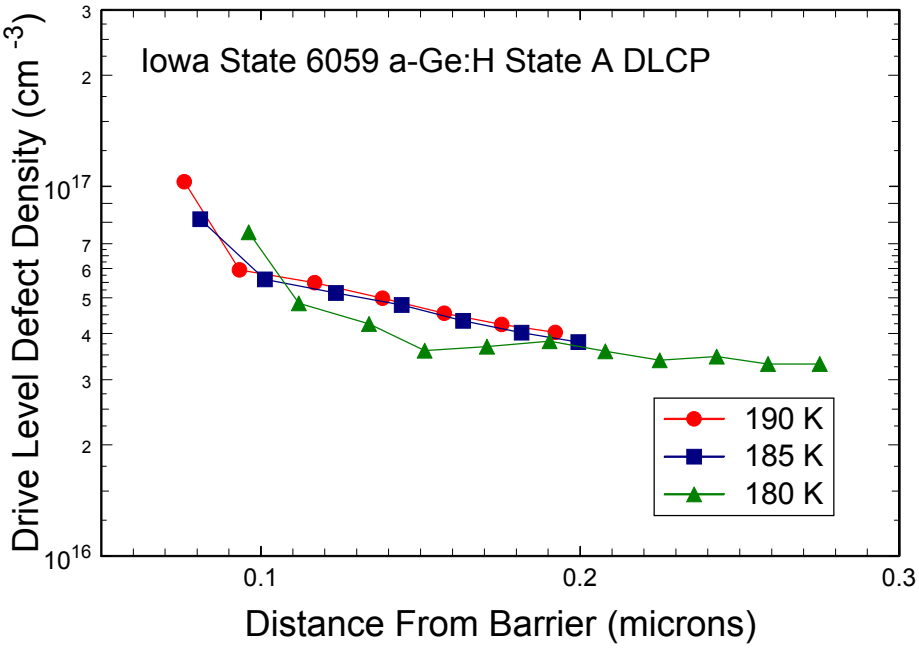

FIG. 3. Drive-level capacitance profiles taken at 330Hz at three measurement temperatures. The defect density indicated is roughly 3.5 x 10^{15} cm^{-3} near the substrate of this a-Ge:H sample. The profiles are nearly temperature independent which indicates that the responding defects must be quite shallow (within 0.4eV of the conduction band mobility edge).

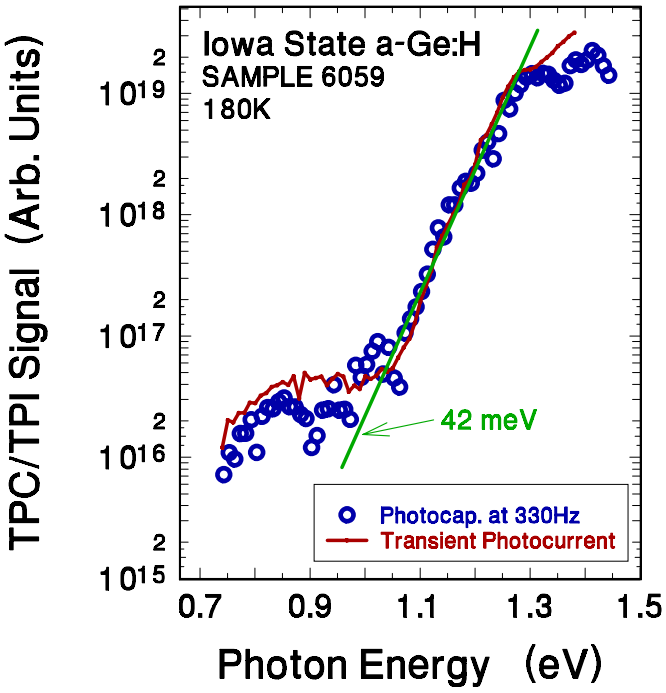

FIG. 4. Transient photocapacitance and transient junction photocurrent spectra for Iowa State a-Ge:H sample 6059. Both spectra indicate an Urbach energy of 42meV, an E_{04} optical gap near 1.3eV, and a deep defect band consistent with the mid 10^{16} cm^{-3} level. This agrees with the DLCP measurements exhibited in Fig. 3.

5.0 PROPERTIES OF UNITED SOLAR NANOCRYSTALLINE SILICON

Simple variations in the growth parameters used to deposit hydrogenated amorphous silicon (a-Si:H) result in the growth of a form of hydrogenated microcrystalline silicon with crystallite sizes less than 10nm: Hydrogenated nanocrystalline silicon, nc-Si:H. Such materials have been studied seriously for solar cell applications for over a decade [12]; however, only fairly recently have attempts to fabricate high efficiency a-Si:H/nc-Si:H tandem cells shown a reasonable degree of success.[13] Compared to a-Si:H, however, the range of materials called micro- or nano-crystalline silicon is enormous. Not only is there the important variable of crystallite size, but also issues such as the degree of a-Si:H contained between the crystallites, the role of hydrogen in passivating grain boundaries, oxygen contamination [14], and the variation of these properties as a function of film thickness [15] are expected to play a crucial role in determining the electronic properties of these materials. We have begun an effort to understand this class of materials. The specific goals include identifying the active defects and understanding their effects, characterizing the carrier densities and transport properties, and identifying under what conditions such materials may exhibit types light-induced degradation similar to a-Si:H. In the preliminary studies reported here, we will discuss some results using admittance spectroscopy, drive-level capacitance profiling, and transient photocapacitance studies on the three samples obtained from United Solar Ovonics Corporation that were described in Section 2 above.

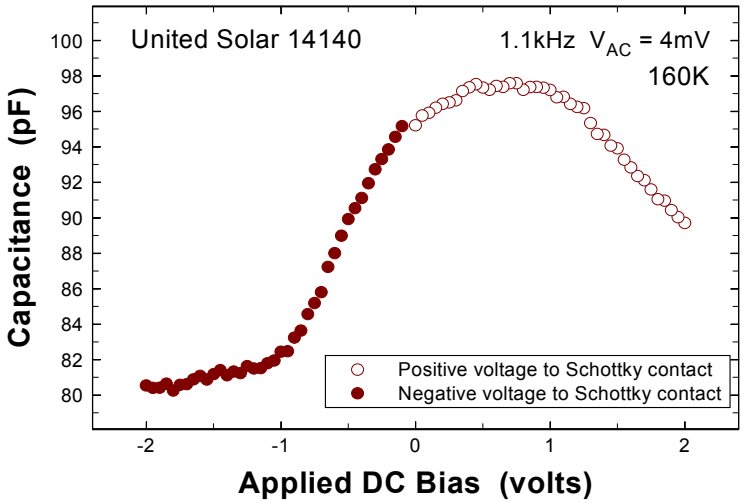

FIG. 5. Variation of the junction capacitance with voltage for the 14140 a-Si:H/nc-Si:H/a-Si:H sandwich sample. These data indicate that blocking contacts probably arise from the a-Si:H/nc-Si:H interfaces on both sides of the nc-Si:H layer. The asymmetry indicates that the effective "built-in potential" is different for the two interfaces. The CV variation is consistent with a doping density close to 10^{15} cm^{-3}.

5.1 ADMITTANCE AND DRIVE-LEVEL CAPACITANCE PROFILING STUDIES

It had been found that nc-Si:H films were susceptible to post-deposition oxygen contamination which could be prevented by depositing capping layers of a-Si:H. Thus, we requested for study an initial sample (14140) that was a 3-layer sandwich consisting of .a 700nm thick nc-Si:H layer clad between two 200 to 250nm thick a-Si:H layers in a SS/n+/a-Si:H/nc-Si:H/a-Si:H structure. We finished our test devices by depositing a Pd Schottky barrier contact on the top surface. In Fig. 5 we display a capacitance voltage measurement for this sample device extending over both forward and reverse biases. These measurements reveal, in spite of the n^+ contacting layer at the substrate, that we actually have blocking contacts for both polarities. We suspect that this behavior occurs as a result of the a-Si:H/nc-Si:H interfaces on both sides of the nc-Si:H layer. The CV dependence indicates an effective doping level of roughly 10^{15} cm^{-3}.

In Fig. 6(a) we display the variation of capacitance with temperature at +0.5V applied bias for a series of seven measurement frequencies. We can see that there are two prominent features: First, there is a large capacitance step lying between 200 and 300K (depending on the frequency). The frequency *vs*. temperature of the inflection point of this capacitance step exhibits Arrhenius behavior as is shown in Fig. 6(b). Initially we thought that this large capacitance step was due to the activation of conduction of the nc-Si:H material. However, the fact that the capacitance below this step varied with applied bias (see Fig. 5) contradicted this interpretation. That is, if conduction in the nc-Si:H became frozen out then we would simply observe a bias independent geometric capacitance at temperatures below the step. We currently believe that, rather than indicating a deep defect level, the capacitance step most likely indicates the onset of participation of states at the nc-Si:H/a-Si:H interfaces to the capacitive response. Such an interface state

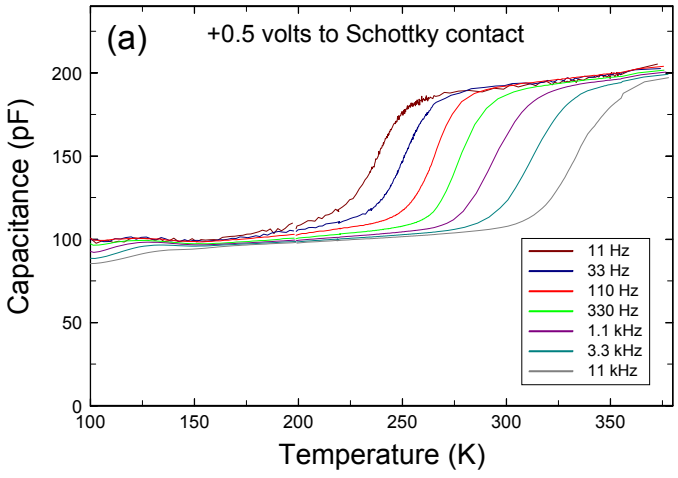

FIG. 6(a). Capacitance vs. temperature for a-Si:H/nc-Si:H/a-Si:H multilayer sample 14140 at +0.5V applied bias and seven measurement frequencies. Note the large capacitance steps at intermediate temperatures (230K to 320K) and the smaller capacitance steps below 130K. The latter is due to dielectric freeze-out of the nc-Si:H layer.

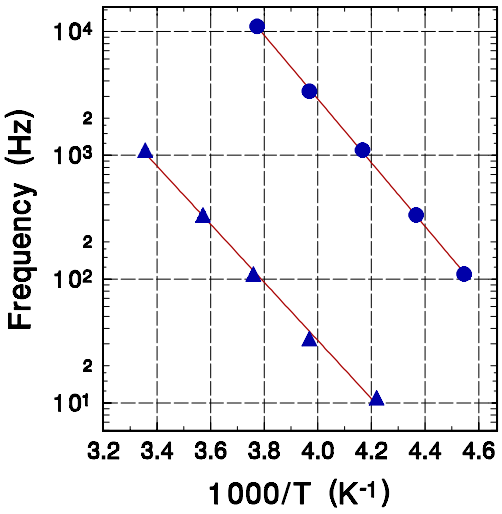

FIG. 6(b). Arrhenius plot of the large capacitance step vs. frequency displayed in Fig. 6(a) (triangles) reveals an activation energy near 0.5eV, close to half the nc-Si:H bandgap We obtain nearly the same activation energy, but very different prefactor, for the p-i-n nc-Si:H sample (circles).

response will often exhibit an activation energy of half the gap, particularly if it arises primarily from minority carrier trapping at such interfaces [16].

We obtained a very similar capacitance step and activation energy for the p-i-n sample 12123 as well [see Fig. 6(b)]. This tends to confirm our interpretation of the step since the thermal generation of carriers will be the same as for the sandwich sample, but the prefactor would be expected to be quite different since it would depend on the density and character of states located in this case at the p-i and/or the n-i interfaces.

The capacitance value in the intermediate temperature region in the sandwich sample is slightly below 100pF, and this corresponds to a total depleted width of roughly 0.9μm. We believe this corresponds to the two a-Si:H layers (roughly 0.5μm) plus a depleted region inside the nc-Si:H layer (of roughly 0.4μm). Below a temperature of roughly 130K we note that the capacitance exhibits another step. Although it is not clear what the asymptotic capacitance value will reach below this step, it appears that it will lie at or slightly below 80pF. This would correspond to a thickness of 1.15μm, or roughly the total thickness of all three layers. Thus, we believe the lowest temperature capacitance step exhibited in Fig. 5(a) actually corresponds to the dielectric freeze-out of conduction in the nc-Si:H layer itself. We note that this appears to occur at quite a low temperature compared to a-Si:H.

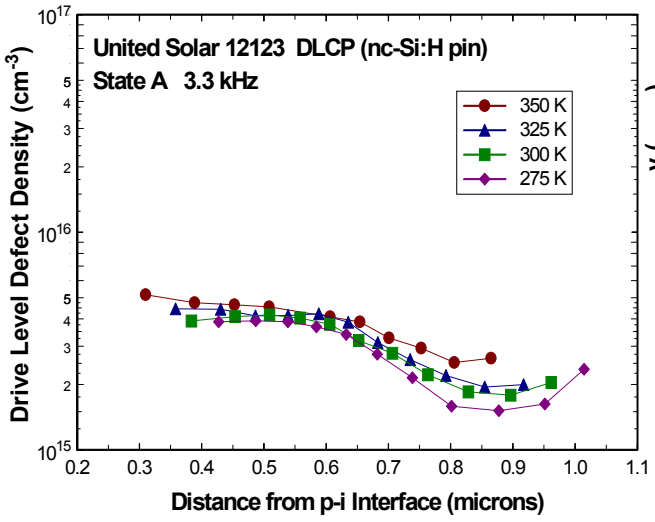

FIG. 7. DLCP curves for the p-i-n nc-Si:H device. Note the small variation of these curves with temperature which indicates that the responding states are relatively shallow.

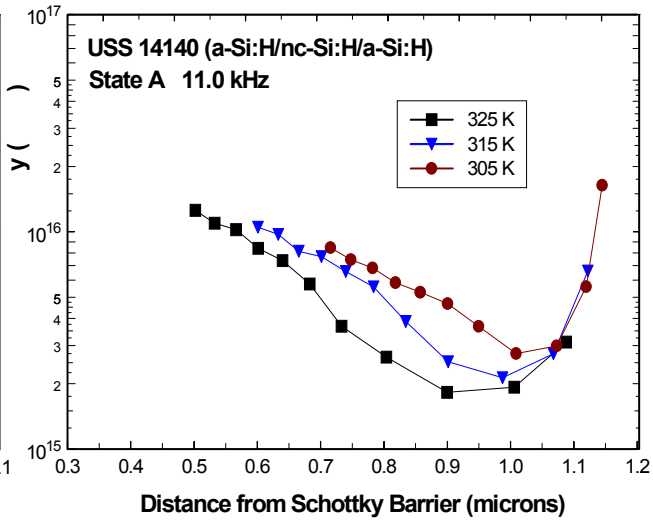

FIG. 8. DLCP curves for the a-Si:H/nc-Si:H/a-Si:H multilayer sample showing a similar qualitative behavior to that of the p-i-n device.

We next characterized these samples using the drive-level capacitance profiling (DLCP) technique. A series of 3.3kHz drive-level profiles for the pin sample device is shown in Fig. 7, and indicates densities near the mid 10^{15} cm^{-3} level. However, the variation of these densities with temperature is quite small. This suggests that the majority of the responding states are shallow donor-like states. A small component of deeper defects may be indicated by the *difference* between the high and low temperature profiles. For this sample we see that any deeper defect density appears to be less than 1 x 10^{15} cm^{-3}. A similar series of drive-level profiles is displayed in Fig. 8 for the multilayer sample. These appear to be qualitatively quite similar to those of the pin device except that they indicate a doping density perhaps twice as large as those for the pin device. For this device there is a larger horizontal shift with varying temperature which is probably due to the increasing response of the a-Si:H layers at temperatures above 300K. If one attempts to correct for this, then the variation of apparent density with temperature becomes much smaller and more consistent with those of the pin device. It is interesting to note in both types of devices that the density becomes substantially smaller as we move toward the substrate part of each device.

5.2 SUB-BAND-GAP PHOTOCAPACITANCE SPECTROSCOPY

In Figures 9 and 10 we display two types of sub-band-gap spectra. The first, in Fig. 9, is a CPM spectrum for hydrogenated microcrystalline silicon (μc-Si:H) taken from the literature [17]. The second, in Fig. 10, is a set of transient photocapacitance (TPC) spectra, taken at three different measurement temperatures, for one of the United Solar nc-Si:H sandwich sample

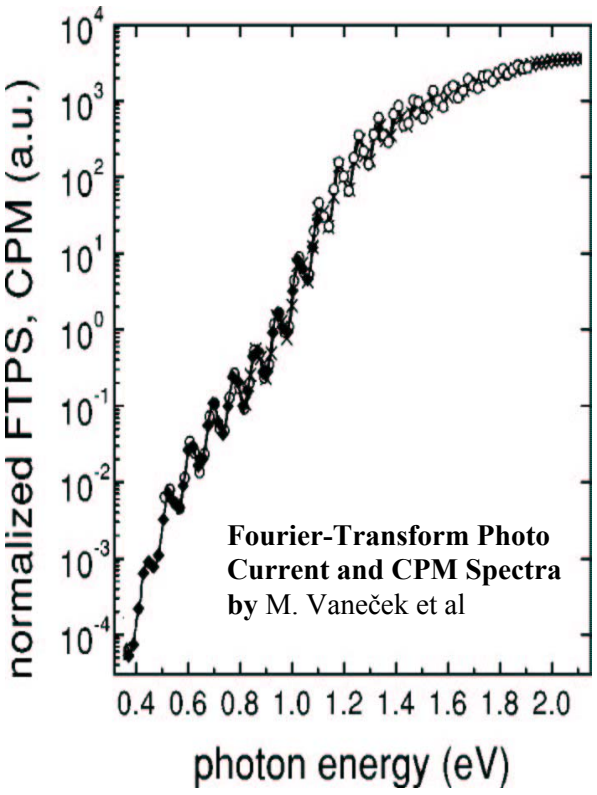

FIG. 9. CPM spectrum for μc-Si:H taken from the paper by M. Vaneček et al [17]. Note the high S/N at low photon energies that was achieved by employing Fourier transform spectrometry.

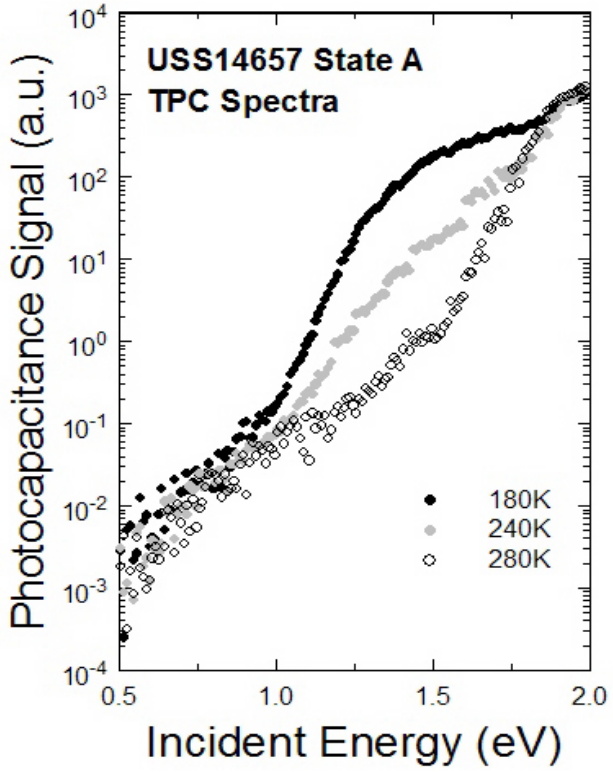

FIG. 10. TPC spectra for one sandwich nc-Si:H sample device at three measurement temperatures. Note that at 180K the spectrum appears very similar to that for μc-Si:H shown in Fig. 9 with similarly good S/N. However, at 280K the spectum appears similar to sub-band-gap spectra for a-Si:H.

devices. It is quite striking that, at the lowest measurement temperature (180K), the TPC spectrum appears quite similar to the CPM spectrum for μc-Si:H, while at the highest measurement temperature (280K), the TPC spectrum appears very similar to what one would expect for hydrogenated *amorphous* silicon!

We believe that the variation in the appearance of the TPC spectra indicates the mixed phase nature of the United Solar nc-Si:H material. Specifically, we believe that the evolution of the appearance of these spectra from being more μc-Si:H like at lower temperatures to more a-Si:H like at higher temperatures is due to the suppression of the nc-Si:H signal component when a majority of minority carriers is able to escape the depletion region during the photocapacitance measurement time window. This cancels the charge change (and hence the photocapacitance signal) caused by the escape of the optically excited majority carriers that is dominant at the lower temperatures. (See the discussion in Section 3.3 above). In contrast, the minority carriers generated in the amorphous silicon component of the sample appear to remain trapped and so this component of the sample dominates the spectrum above 280K.

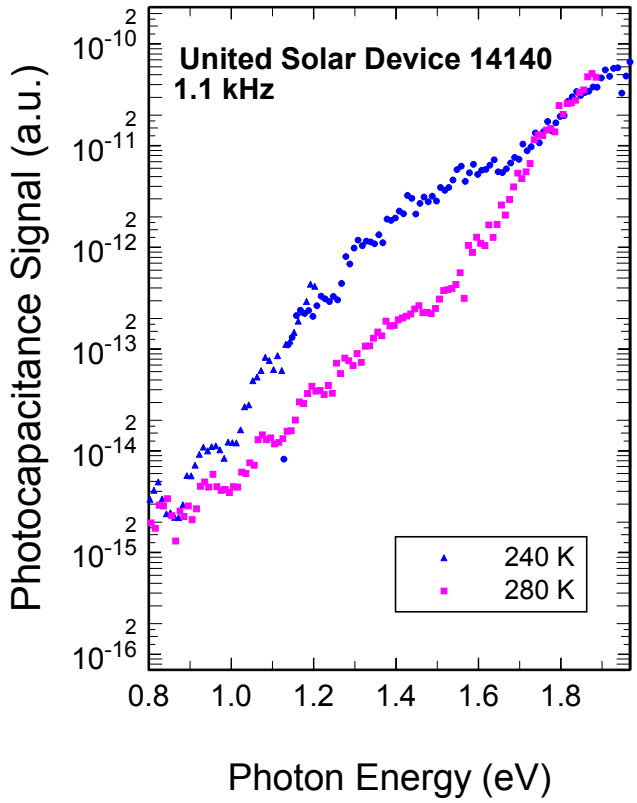

FIG. 11. Photocapacitance spectra for one a-Si:H/nc-Si:H/a-Si:H multilayer sample at two measurement temperatures. The spectra indicate both nc-Si:H and a-Si:H components.

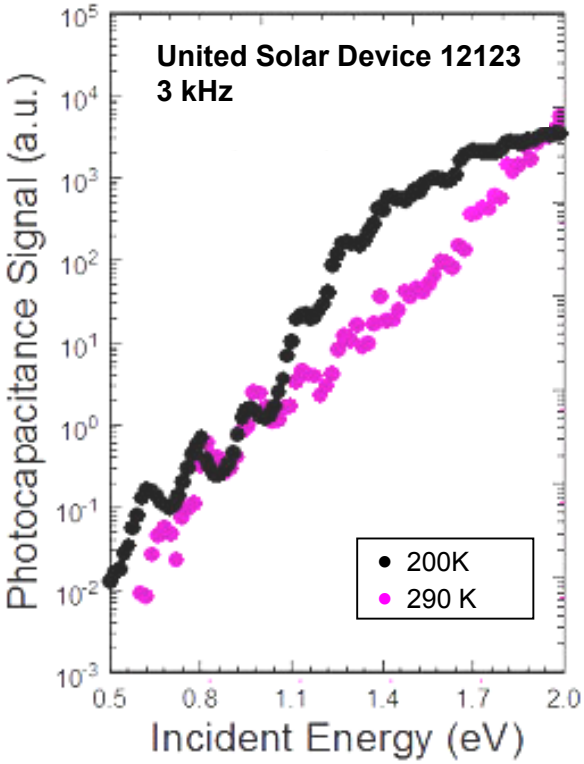

FIG. 12. Photocapacitance spectra for the pin nc-Si:H device at two measurement temperatures. Note the similar appearance to that of the multilayer device of Fig. 11.

Initially we were not certain whether the a-Si:H component of the signal in Fig. 10 came from the nc-Si:H layer itself or from the a-Si:H layers of this multilayer device. The latter possibility did not seem likely at these low measurement temperatures since the conductivity in the a-Si:H layers would be too low to respond to a kHz oscillating voltage. In Figures 11 and 12 we compare TPC spectra for the second sandwich sample with the purely nc-Si:H pin device. We see that both exhibit very nearly the same type of temperature dependence. Therefore, the fact that the pure nc-Si:H device exhibits qualitatively the same type of spectra confirms that the a-Si:H component of these spectra arises because the United Solar nc-Si:H material is a composite containing a significant fraction of a-Si:H. This conclusion has recently been verified by XRD measurements on similar United Solar nc-Si:H films.[18]

5.3 LIGHT INDUCED EFFECTS IN MICROCRYSTALLINE SILICON

Although it has been reported that nc-Si:H is largely immune from the light induced degradation effects exhibited by a-Si:H [14, 19], recent studies on the performance of nc-Si:H

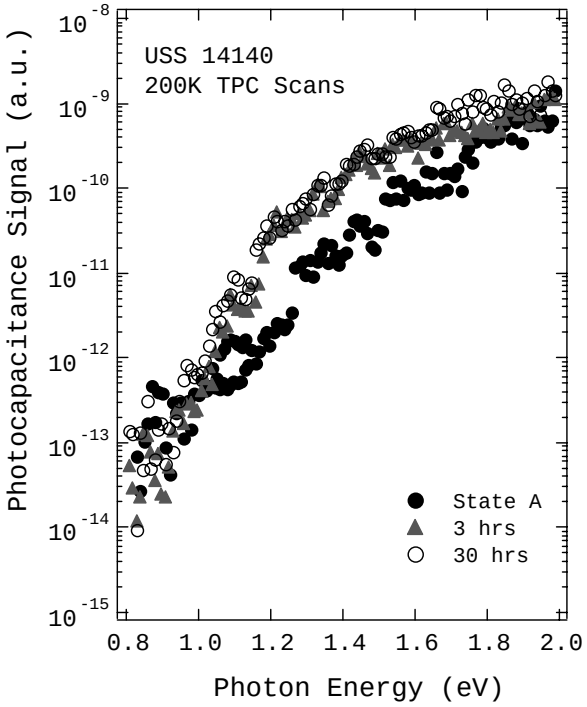

FIG. 13(a). Comparison of 200K photocapacitance spectra in State A and after 2 periods of light soaking. We believe that the increase in the magnitude arises primarily from a decrease in the hole carrier collection.

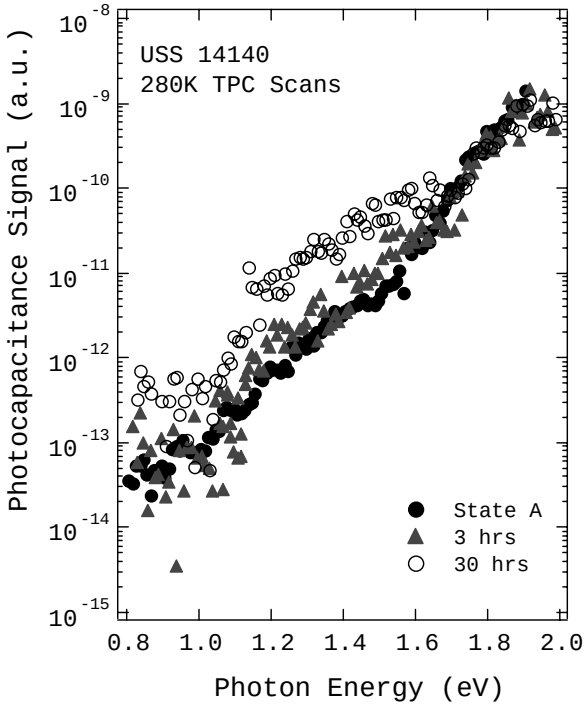

FIG. 13(b). Comparison of 280K photocapacitance spectra in State A and after 2 periods of light soaking. Note the continued increase in the nc-Si:H signal component of these spectra after 30 hours of exposure.

solar cell devices fabricated at United Solar [20] have revealed a 7 to 10% loss in efficiency after prolonged exposure. However, as mentioned above, no evidence for changes in the electronic properties have been found thus far in our admittance or DLCP measurements. In Fig. 13(a) we display a series 200K TPC spectra for sample 14140 in State A and after 3 and 30 hours of light soaking, with red filtered (610nm) ELH light at 100mW/cm^2 intensity. At this temperature the nc-Si:H spectral response is clearly the dominant component that is observed.

This series of spectra clearly shows a significant change (an increase in magnitude) after the initial 3 hours of light soaking, but very little change after that. According to the discussion in the previous section, we believe that this change reflects a decrease in the minority carrier collection. Furthermore, although little change is observed beyond 3 hours of light soaking at 200K, continuing changes are evident if we increase the temperature [see spectra recorded at 280K displayed in Fig. 13(b)]. That is, the hole collection fraction is reduced to a level too low to easily detect after 3 hours of light soaking in our 200K measurement. However, the hole collection fraction becomes larger with increasing temperature (see Fig. 10) so that we can observe a continuing loss in hole collection at longer light soaking times in the higher

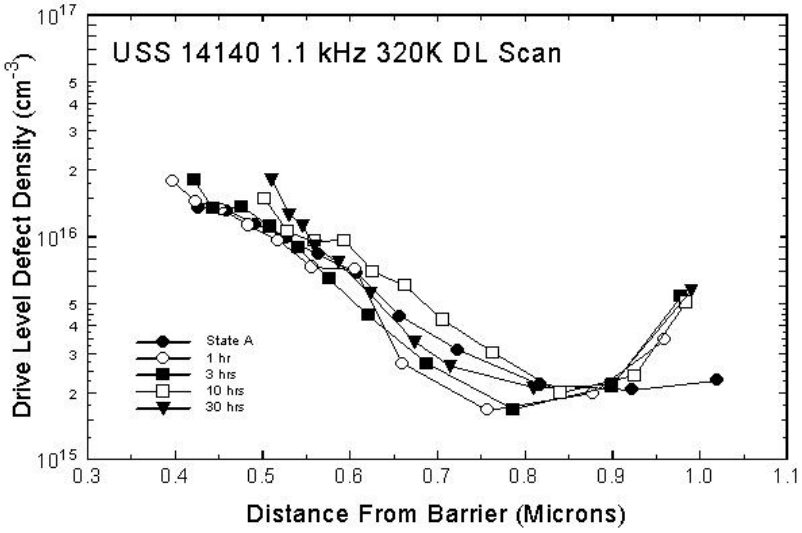

FIG. 14. Drive-level capacitance profiles taken at 1.1kHz and 320K for State A and the various stages of light soaking indicated. These densities exhibit only relatively minor changes with light exposure and probably primarily reflect the effective doping level within the nc-Si:H component of the sample.

temperature measurements. Indeed, by increasing the temperature to 320K we continue to observe a decrease in the hole collection even after 100 hours of light soaking. At the present time we are unable to propose any particular change in the electronic structure that may be responsible, although Fig. 13(b) suggests that there may be an increase of the deep defect band of these spectra a result of light soaking.

Finally, in Fig. 14, we display the results of drive-level capacitance profiling (DLCP) measurements on this sample in State A, and after 1, 3, 10, and 30 hours of light soaking. In these profiles very little change is observed. However, typically under the experimental conditions employed (1.1kHz and 320K) these measurements would only be sensitive to defect states shallower than about 0.60eV. Therefore, these would miss any response from deep states within the a-Si:H component. Instead these profiles probably mostly reflect the shallow states of the nc-Si component that give it its n-type character. This effective doping level is apparently only very slightly modified by whatever light-induced changes are taking place.

6.0 SUMMARY AND CONCLUSIONS

During this second phase of our NREL Subcontract period we have focused primarily upon the characterization of hydrogenated nanocrystalline Si (nc-Si:H) produced at United Solar Ovonics Corporation. We applied both drive-level capacitance profiling (DLCP) and transient photocapacitance (TPC) spectroscopy for this purpose, and this year's annual report gives our first results of this material. In addition, we examined a couple of amorphous germanium (a-Ge:H) samples produced by the ECR method at Iowa State University. Our studies in the latter case confirmed the superior electronic properties of the Iowa State a-Ge:H material, both in terms of the DLCP deduced defect densities, and the TPC deduced Urbach energies.

In our DLCP studies of the nc-Si:H we found responding state densities in the 10^{15} to 10^{16} cm^{-3} range. However, very little temperature dependence was observed, indicating that the majority of these are shallow donor-like states. For all 3 samples studied (two sandwich samples with capping a-Si:H layers as well as one purely nc-Si:H p-i-n device) we observed that the DLCP densities increased in the direction of film growth. This is consistent with observations at USOC that the crystallinity size increases as the films become thicker. We are not certain at this point whether this increasing DLCP density with thickness indicates an increasing density of deep defects, or merely an increasing shallow donor density. Future work on nc-Si:H samples with intentional hydrogen profiling during growth to maintain a more constant crystallite size should help provide some additional insight into these issues.

The most informative studies of the nc-Si:H material, however, were based upon our TPC spectroscopic measurements. Here, much to our surprise, we found that the TPC sub-band-gap evolved from an appearance that agreed quite well at lower temperatures (200K) with previous sub-band-gap spectroscopic studies on μc-Si:H using methods such as CPM, but became very a-Si:H like in appearance at moderate temperatures (300K). This change in appearance is believed to be a result of improving hole carrier collection as the temperature is increased which then diminishes the photocapacitance response of the nc-Si:H component in these materials. However, there is also an a-Si:H component in these nc-Si:H samples in which the hole carrier collection remains relatively poor even as the temperature is increased. The TPC signal in that component thus becomes dominant in the higher temperature regime even though its volume fraction is undoubtedly fairly small. These results agree with recent x-ray diffraction measurements taken by Don Williamson on the USOC nc-Si:H material [20]. More precise quantitative estimates of the volume fractions involved, as well as the fraction of holes collected in each component as a function of temperature, may be possible after we collect comparison transient photocurrent (TPI) spectra for these samples over an extended temperature range.

Finally, we have begun to examine the effects of light-induced degradation in these nc-Si:H materials. The DLCP measurements actually showed very little change with light soaking, even after 100 hours at $100mW/cm^2$. However, significant degradation in the hole carrier collection properties were observed in the TPC measurements. That is, as the degradation time was increased we found that the TPC nanocrystalline signal increase monotonically, indicating a monotonic decrease in the fraction of minority carriers escaping from the depletion region. However, we did not observe any increase in any specific spectral feature or defect band that might provide a clue for a mechanism that might be responsible for this loss of hole collection. Examining the effects of light-induced degradation in more detail will certainly be a focus of our work in the upcoming Subcontract year.

7.0 SUBCONTRACT SUPPORTED PUBLICATIONS

1. J. David Cohen, "Light-induced defects in hydrogenated amorphous silicon germanium alloys", Sol. Energy Mat. and Solar Cells **78**, 399 (2003).
2. J. David Cohen, "Metastable defects in the amorphous silicon-germanium alloys", Mat. Res. Soc. Symp. Proc. **762**, 51 (2003).

8.0 REFERENCES

1. Yong Liu and Vikram L. Dalal, Mat. Res. Soc. Symp. Proc. **715**, 515 (2002).
2. D.V. Lang, J.D.Cohen, and J.P. Harbison, Phys. Rev. B**25**, 5285 (1982).
3. C.E. Michelson, A.V. Gelatos, and J.D. Cohen, Appl. Phys. Lett. **47**, 412 (1985).
4. K.K. Mahavadi, K. Zellama, J.D. Cohen, and J.P. Harbison, Phys. Rev. B**35**, 7776 (1987).
5. J.D. Cohen and A.V. Gelatos, in *Advances in Disordered Semiconductors Vol I: Amorphous Silicon and Related Materials*, ed. by H. Fritzsche (World Scientific, Singapore, 1988), pp. 475-512.
6. J. David Cohen, Thomas Unold, A.V. Gelatos, and C.M. Fortmann, J. Non-Cryst. Solids **141**, 142 (1992).
7. T. Unold, J.D. Cohen, and C.M. Fortmann, Mat. Res. Soc. Symp. Proc. **258**, 499 (1992).
8. A.V. Gelatos, K.K. Mahavadi, and J.D. Cohen, Appl. Phys. Lett. **53**, 403 (1988).
9. Chih-Chiang Chen, Fan Zhong, J.D. Cohen, Jeffrey C. Yang, and Subhendu Guha, Phys. Rev. B**57**, R4210 (1998).
10. D. Kwon, C.-C. Chen, and J.D. Cohen, H.-C. Jin, E. Hollar, I. Robertson, and J.R. Abelson, Phys. Rev. B**60**, 4442 (1999).
11. Paul Wickboldt, Dawen Pang, William Paul, Joseph H. Chen, Fan Zhong, Chih-Chiang Chen, J.David Cohen, and Don L. Williamson, J. Appl. Phys. **81**, 6252 (1997).
12. J. Meier, R. Flückiger, H. Keppner, and A. Shah, J. Appl. Phys., **65**, 860 (1994).
13. See, for example, Y. Tawada, H. Yamagishi and K. Yamamoto, Sol. Energy Mat. and Sol. Cells, 78, 647 (2003).
14. P. Torres, J Meier, R. Flückiger, U. Kroll, J. A. Anna Selvan, H. Keppner, and A. Shah, J. Appl. Phys., **69**, 2286 (1996)
15. B. Yan, G. Yue, J. Yang, S. Guha, D. L. Williamson, D. Han and C.S. Jiang, Mat. Res. Soc. Symp. A, 2004, to be published
16. See, for example, H-R. Park, D. Kwon, and J.D. Cohen, J. Appl. Phys. **83**, 8051 (1998).
17. M. Vaněček and A. Poruba, Appl. Phys. Lett. **80**, 719 (2002).
18. Baojie Yan, private communication.
19. A.V. Shah, J. Meier, E. Vallat-Sauvain, N. Wyrsch, U. Kroll, C. Droz, U. Graf, Sol. Energy Mat. Sol. Cells, **78**, 469 (2003)
20. B. Yan, G. Yue, J. Yang, S. Guha, D. L. Williamson, D. Han and C.S. Jiang, Mat. Res. Soc. Symp. A, 2004, in press.